ACS Photonics

Open Access

This article is licensed under CC-BY 4.0

pubs.acs.org/journal/apchd5

Article

Statistically Identified Dual Type Random Lasing from Carbon Dots

Ashim Pramanik, Marco Reale, Marco Cannas, Radian Popescu, Alice Sciortino, and Fabrizio Messina*

Cite This: https://doi.org/10.1021/acsphotonics.4c00279

Read Online

ACCESS | Metrics & More | Article Recommendations | Supporting Information

ABSTRACT: Random lasers (RLs) attract a growing interest in photonics as laser-like sources featuring specific benefits over traditional lasers for some applications. Carbon dots (CDs) are well-recognized as one of the most appealing fluorescent nanomaterials for light emitting devices. However, achieving unambiguous and controllable RL emission from CDs remains challenging. Here, we demonstrate RL emission at ∼565 nm from green emitting CDs (gCDs), and we use the emitted light as a light source for the speckle-free microscopy of biological tissues and microparticles. The emission of the CD-based RL is thoroughly studied as a function of the experimental conditions, and well-established mathematical tools in the field are used to perform a detailed statistical study of the lasing output. The CD-based RL displays ultranarrow (∼0.70 nm) emission lines over a comparatively broader (∼10 nm) background. These two emissions are due to the so-called coherent and incoherent RL. Their relative weight can be controlled by an appropriate choice of experimental conditions, allowing us to tune the characteristics of RL light. The results demonstrate the potential of gCDs as a viable alternative to environmentally unfriendly, scarce, or chemically unstable nanomaterials as gain media for RL with customizable emissions.

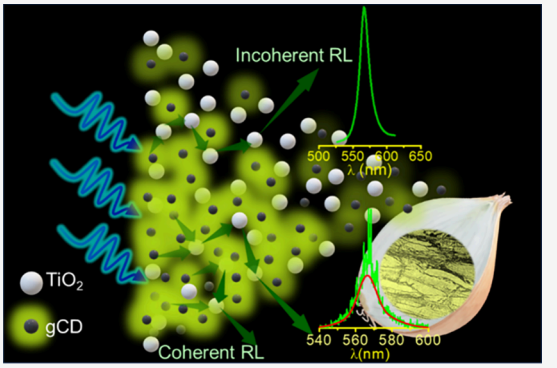

KEYWORDS: *carbon dots, optical gain, random laser, statistical analysis, speckle free imaging*

Downloaded via KIT BIBLIOTHEK on August 1, 2024 at 13:30:55 (UTC).
See https://pubs.acs.org/sharingguidelines for options on how to legitimately share published articles.

INTRODUCTION

Random lasers (RLs) are an emerging family of mirrorless laser-like light sources with foreseeable impact in next-generation photonic technologies, considering their simplicity in terms of design, low cost, and adjustable spatial coherence.[1−3] Unlike other lasers, where coherent narrowband light emission is achieved by coupling the gain medium to an optical resonator, RLs exploit the commonly observed phenomenon of light scattering inside a disordered structure.[4] Typically, a colloidal dispersion of fluorescent nanoobjects, behaving as photonic gain media, is mixed with passive scatterers, and the blend can lead to an intense omnidirectional narrow-band laser-like emission if pumped over a certain threshold energy.[5] Alternatively, the same nanoobject can serve both as emitter and scatterer.[6,7] Generally, we can discriminate two types of RL: coherent and incoherent. Incoherent RL occurs when emission is amplified by a chain of nonresonant scattering events before leaving the medium.[4] Scatterers dramatically increase the optical path inside the medium, thus favoring light amplification. In contrast, coherent-type RL can stem from at least two different mechanisms: highly efficient scattering events determining the formation of closed "loops", which effectively act as well-defined microcavities,[8,9] or the formation of extended modes characterized by very long light paths, capable of large amplification even through a nonresonant mechanism.[10,11] Coherent RL emission is advantageous for medical diagnostics,[12,13] random number generation,[14,15] photonic barcodes,[16] and super resolution spectroscopy.[17] In contrast, the low spatial coherence of incoherent RL is appealing for speckle-free imaging applications.[3,18] The two RL types can also coexist,[19] and their relative weight is controlled by experimental parameters such as the concentration of scatterers and pumping conditions. The interplay between coherent and incoherent RL leads to intricate statistical properties of the emitted light which are theoretically interesting in photonics and physics of complex systems.[10,19,20]

Several possible combinations of gain media (fluorescent dyes or nanosystems) and scatterers have been explored in the design of RLs. For example, cadmium-based quantum dots (QDs) or luminescent halide perovskites are good candidates for lasing and random lasing, as shown by several literature examples.[21,22] However, the inherent instability and narrow optical tunability of perovskites, the severe toxicity of perovskites and QDs, and the severe photobleaching of most fluorescent dyes practically limit the adoption of these materials for stable and low-threshold RL.[23] Therefore, one

Received: February 13, 2024
Revised: May 9, 2024
Accepted: May 9, 2024

© XXXX The Authors. Published by American Chemical Society

of the key challenges of the field is to develop environmentally friendly, water-soluble, and photostable luminescent nanomaterials for easily accessible photonic applications based on RL.

In the last two decades, carbon dots (CDs) have been emerging as a candidate nanomaterial for bioimaging and optoelectronic applications because of their bright tunable fluorescence.[24,25] Broadly speaking, CDs can be seen as a carbon-based equivalent of quantum dots (QDs), endowed with specific advantages due to their water solubility, ease of functionalization, and lack of rare or critical chemical elements.[26,27] CDs have been applied in light-emitting devices ranging from electroluminescent white-light emitting diodes[28−30] to more exotic latent fingerprint detection devices.[31] In regard to lasers, although CD optical gain coefficients are generally smaller[32,33] than luminescent dyes, QDs, and perovskites,[34−36] CDs have been successfully used as gain media in traditional laser cavities.[37,38] However, CD-based random lasers remain challenging, since CDs are usually quenched by semiconductor or metal nanoscatterers.[39,40] Thus, only a few works have provided clear-cut evidence of paradigmatic mirror-free RL emission from a mixture of CDs and metal or semiconductor scatterers.[41,42] Other works have rather demonstrated hybrid designs, where RL is observed from CDs hosted inside a microresonator under certain experimental conditions,[43] or scatterers[38] are utilized to reduce CD lasing threshold within a Fabry−Perot cavity. While lasing from CDs housed inside a square cuvette easily leads to directional laser beams,[44,45] it is often unclear if this emission can be classified as Fabry−Perot lasing off cuvette walls, which can provide remarkably strong feedback even without external mirrors, or rather RL enabled by scattering from CDs themselves. In general, discriminating true RL from other forms of laser amplification and pinpointing the transition from incoherent to coherent RL can be difficult tasks that can only be achieved by a thorough analysis of the statistical properties of the emitted light, by analyzing shot-by shot fluctuations of the narrowband emission, and by comparing the characteristics of the emissions in various pumping geometries. This type of study has hardly been conducted on CD-based RLs despite being mandatory to fully optimize them for applications.

Here, we demonstrate RL emission from green emitting CDs (gCDs) in the presence of TiO_2 nanoparticles used as scatterers. The fingerprint of RL is a drastic narrowing of gCD emission in the presence of scatterers, ultimately yielding highly omnidirectional and stable RL emission peaking around 565 nm. We thoroughly analyze the statistical properties of RL emission and determine key quantities such as the threshold pump energy and gain coefficient. Importantly, we demonstrate that the system undergoes a transition from an incoherent to coherent RL when the gCD concentration overcomes a defined threshold. Finally, we demonstrate the use of generated RL emission as an illumination source for speckle-free imaging. The results pave the way to using gCDs as a viable gain medium for achieving customized RL emissions from a single type of disordered system.

EXPERIMENTAL SECTION

Preparation of gCDs. The synthesis of gCDs is conducted by hydrothermal decomposition of organic precursors, as reported in our previous works.[46,47] Shortly, urea (3 g) and citric acid monohydrate (3 g) (Sigma-Aldrich) are mixed to prepare the precursor solution in 10 mL of Milli Q water. This solution is heated over a hot plate until the solvent completely evaporates. As a result, a dark substance is obtained, which is converted to a fine-grained powder using a mortar. Prior to the RL experiment, the as-synthesized gCD powders were dispersed in DI water and centrifuged at 10000 rpm for 15 min to separate the bulk aggregates. Thereafter, the as-synthesized gCD sample is structurally and optically characterized prior to the RL experiment.

Structural Characterization of gCDs. Attenuated total reflection (ATR) spectra of gCDs are measured in the range of 4000 to 400 cm^{-1} by using a Bruker Platinum ATR spectrometer equipped with a single reflection diamond crystal. High-resolution transmission electron microscopic (HRTEM) images of the gCDs are collected on an aberration-corrected FEI Titan 380−300 microscope operating at 300 keV electron energy. Prior to the HRTEM measurement, the as prepared gCD sample is deposited on a holey carbon-film copper grid at room temperature in air.

Steady-State and Transient State Optical Characterization of gCDs. Optical absorption spectra of gCDs and TiO_2 are measured in 1 cm cuvettes by using an Avantes Star Line ULS2048CLEVO optical fiber spectrometer working in the range 200−1300 nm using a dual deuterium/halogen lamp as a broadband light source. Photoluminescence (PL) decay kinetics of the gCDs in aqueous dispersion (loaded inside a 1 mm cuvette) are measured by using an intensified CCD camera (PI-MAX Princeton Instruments, Trenton, NJ) synchronized to the pump source, i.e., a wavelength tunable optical parametric oscillator pumped by a Q-Switched Nd:YAG laser (OPOTEK VIBRANT, λ_{ex} = 435 nm, 5 ns, 10 Hz). PL lifetimes (τ) were extracted by least-squares fitting the temporal kinetics of the peak emission intensity with single-exponential functions. Emission quantum yields (QY) were estimated by comparing the emission intensity with a reference dye dispersion (Fluorescein, water, pH 11) with known QY = 0.95. Femtosecond transient absorption (TA) measurements aqueous dispersions of gCDs excited at 400 nm were carried out in a home-built experimental femtosecond pump−probe setup described before.[46,47] The latter is based on a 5 kHz Ti:sapphire femtosecond amplifier (Spectra Physics Solstice-Ace) producing 75 *fs* pulses peaking at 800 nm (full width at half-maximum = 30 nm) with 3.50 mJ energy/pulse.

RL Experiments. In the RL experiment, we have used the as synthesized gCDs as gain media and commercial TiO_2 nanoparticles (diameter ∼34 nm, AEROXIDE TiO_2 P90) as passive scatterers. The two components were dissolved together in Milli-Q water in variable concentrations and tested for RL emission under high power pulsed excitation. A tunable pulsed laser system (5 ns, 10 Hz, OPOTEK VIBRANT) is used as the pump source. The pump beam at 435 nm passed through an aperture of diameter 7 mm and then focused on the sample using a plano-convex cylindrical lens (f = 50 mm). The active RL medium, consisting of mixed TiO_2-gCD aqueous suspensions, was contained inside a square or triangular cuvette placed slightly away from the focal point of the lens. In particular, triangular cuvettes allow to avoid external cavity effects due to reflections from cuvette walls. The spectral shape of the light emitted from the RL medium was recorded at different pump energies (E_{in}) using an optical fiber (numerical aperture 0.22) connected to (i) a one-box spectrometer (Thorlabs, CCS200) with a spectral resolution of <2 nm, or (ii) a detection system consisting in a monochromator with 0.15 nm spectral resolution dispersing over an intensified CCD camera (PI-MAX Princeton Instruments) synchronized to the

https://doi.org/10.1021/acsphotonics.4c00279
ACS Photonics XXXX, XXX, XXX−XXX

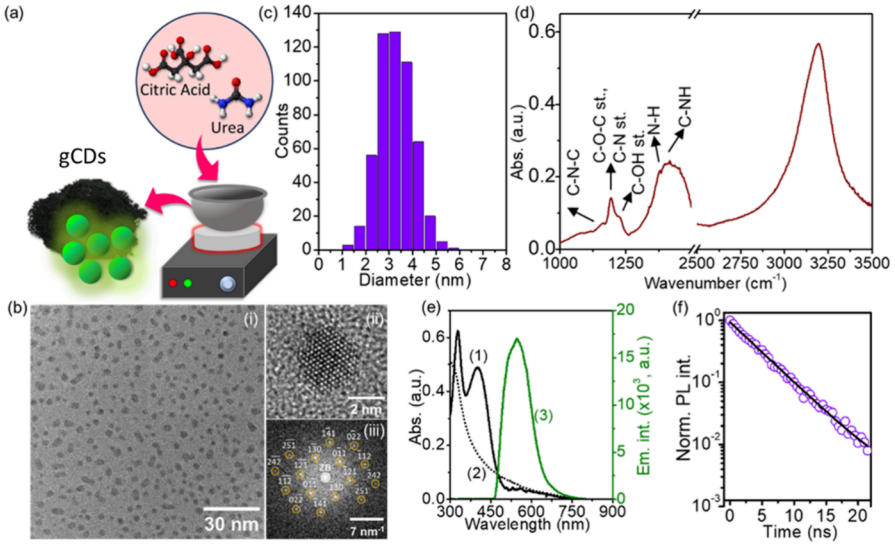

Figure 1. Structural and optical properties of gCDs. (a) Schematic depicting of the synthesis of gCDs from organic precursors. (b) (i) TEM image of gCDs, and (ii) HRTEM image of a single gCDs (~3.4 nm) with β-C_3N_4 crystalline core, as inferred from the corresponding 2D FFT pattern (iii). (c) Size distribution of gCDs as extracted from the TEM image shown in (b(i)), which consist of ~530 nanoparticles. (d) IR absorption spectrum of gCDs; the attributions of the IR signals are indicated by the arrows. (e) UV−vis extinction spectra of (1) gCD and (2) TiO_2 (~34 nm), and (3) PL emission spectrum of gCDs (λ_{ex} = 435 nm). (f) Normalized emission decay profile (violet points) of gCD, and the corresponding least-squares fitting (black line) of the data with a single exponential decay function. The excitation wavelength used for the photoluminescence measurements in panels (e) and (f) is 435 nm.

pump source. Use of the latter detection system allowed both to achieve higher spectral resolution and perform time-resolved measurements. RL experiments were performed on disordered systems containing (i) different number densities of scatterers ($N_{sc} \approx 4.30$ to 8.70×10^{14} cm^{-3}) and (ii) two different concentrations of gCDs having a fixed N_{sc} of $\sim 8.70 \times 10^{14}$ cm^{-3}. Henceforth, gCD dispersions prepared in two different concentrations are denoted as gCD1 (~2 g/L) and gCD2 (~4 g/L).

Speckle-Free Imaging. We tested the RL beam as a source for imaging in a microscopy setup. Experiments were conducted on a standard microscopy test pattern (THORLABS, R1L3S10P - Positive NBS 1952 Resolution Target), on an *Allium cepa* cell membrane, and on a sample of polystyrene microparticles (~3 μm, Polysciences, Inc.) deposited on a glass substrate. To do this, the RL emission was transported to an optical microscope (MOTIC, BA300) by using a multimode round fiber optic bundle cable (THORLABS), the exit of which was fixed at the point of illumination. Then, the samples to be imaged were placed in the microscope with the help of stage clips, and a CCD camera (THORLABS, Zelux, CS165MU1/M) was fixed at the trinocular port of the microscope for collecting the images through the 4× objective lens of the microscope.

RESULTS AND DISCUSSION

Structural and Photophysical Properties of gCDs as Gain media. A simple liquid phase pyrolysis of citric acid and urea described in the Materials section is carried out to synthesize gCDs, as schematically presented in Figure 1a and already reported in our previous works.[46,47] Typical characterization results of gCDs are shown in Figure 1b,c, demonstrating the formation of carbon dots with a diameter distribution peaking at about 3.3 ± 0.7 nm, as found from transmission electron microscope (TEM) images (Figure 1b(i)). These gCDs host a crystalline β-C_3N_4 core, as demonstrated by the HRTEM image and corresponding fast-Fourier-transform (FFT) analysis shown in Figure 1b(ii−iii), as discussed in detail in our previous report.[46]

Their surface structure was characterized by the ATR absorption data shown in Figure 1d. The absorption peaks at ~1160, 1190, and 1226 cm^{-1} correspond to stretching vibrations of C−N−C, C−O−C/C−N, and C−OH bonds, respectively,[48−50] while the peaks at ~1375 and 1416 cm^{-1} are related to the bending vibrational modes of N−H and C−NH groups.[51,52] The unresolved IR absorption extending from ~3000 to 3430 cm^{-1} is related to the stretching vibrations of OH and NH groups.[53] Overall, the presence of surface hydroxyl, carboxyl and amino functional groups are responsible for hydrophilicity and stability of gCDs in water.[54]

Three main absorption bands can be observed in the UV−vis spectrum of aqueous gCD suspensions (Figure 1e). The absorption peak at ~250 nm corresponds to transitions within the crystalline core.[55] The absorption band centered at ~330 nm is either due to $n \rightarrow \pi^*$ transition originated from surface carboxyl moieties (C═O)[28] or to transitions localized on small molecular moieties embedded in the structure of the CDs.[56] The low-energy transitions centered at ~400 nm, with a long tail at lower energy, are quite common CDs with high nitrogen content,[28,57] which are known to display very efficient visible-light emission.[58] The emission spectrum of gCDs collected at an excitation wavelength of 435 nm is shown in Figure 1e, and it consists of a single emission band centered at ~535 nm. Additionally, absorbance of gCDs increases with concentration without significant changes of shape (Figure S1a), which rules out aggregation, even at the highest explored concentration. Similarly, the PL emission intensity increases considerably with increasing gCD concentration up to ~4g/L, after which it becomes saturated due to the effect of photo reabsorption (Figure S1b). The PL quantum yield (QY) is estimated to be ~12% in water. PL decay kinetics of the gCDs were measured at an excitation wavelength of 435 nm, as

https://doi.org/10.1021/acsphotonics.4c00279
ACS Photonics XXXX, XXX, XXX−XXX

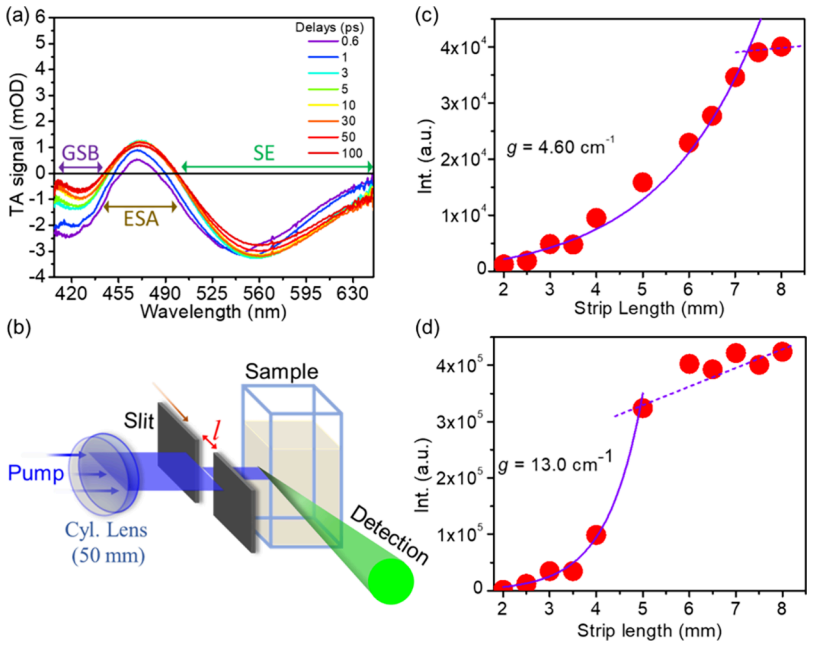

Figure 2. Suitability of gCDs as gain medium for RL emission. (a) Femtosecond time-resolved transient absorption (TA) spectrum of gCDs recorded at variable delays after photoexcitation. GSB, ESA, and SE labels indicate ground-state bleaching, excited-state absorption, and stimulated emission contributions to the TA signal, respectively.[47] (b) Schematic of the VSL experiment to estimate the gain coefficient. Dependence of output emission intensity on the variable excitation-length for the aqueous dispersions of (c) gCD1 (~2 g/L) and (d) gCD2 (~4 g/L). Fitting of the experimental data allows one to estimate the gain coefficient of gCDs at the two different concentrations.

shown in Figure 1f. The PL lifetime (τ) extracted from these data is 4.5 ± 0.2 ns. These data were collected at a concentration of ~2 g/L (hereafter referred to as gCD1). The value of τ slightly decreases to ~3.6 ± 0.2 ns when the concentration of gCDs increased up to 4 g/L (gCD2), as shown in Figure S2a (Supporting Information), suggesting the onset of collisional self-quenching at higher concentrations.

As a starting point for our lasing experiments, key parameters such as spontaneous emission cross section (σ_{em}, in cm^2) and gain coefficient (g, in cm^{-1}) were estimated to evaluate the gCDs' performance as gain medium for amplified spontaneous emission (ASE) and lasing. The value of σ_{em} for gCDs can be estimated from the following relation:[59]

$$\sigma_{em}(\lambda) = \frac{\lambda_4^e E_0(\lambda)}{8\pi c n^2 \tau_r} \quad (1)$$

where $E_0(\lambda)$ is the normalized emission profile, $\tau_r = 1/k_r = \tau/QY$ is the radiative lifetime, c is the speed of light, and n is the refractive index of the surrounding medium (water). The radiative lifetime was estimated from the measured lifetime and QY reported above, as $\tau_r = \tau/QY \approx 37.5$ ns. The extracted value of σ_{em} calculated from eq 1 at peak emission wavelength is ~1.2×10^{-17} cm^2. This estimate is suggestive of a strongly dipole-allowed emission transition, alike to other common laser gain materials,[60] suggesting that luminescent gCDs may have potential application for lasing. We also performed femtosecond transient absorption (TA) measurements on aqueous dispersions of gCDs, excited by 90 fs pulses at 400 nm. TA data shown in Figure 2a clearly depict a strong negative contribution within a broad spectral range of 500 to 650 nm, due to stimulated emission (SE). As expected from a high quantum yield system, the TA signal displays little evolution at variable delays from photoexcitation, except for a small progressive redshift of the SE band due to progressive solvation relaxations. The SE in Figure 2a peaks around 565 nm, which is slightly different from the fluorescence peak at 530 nm visible in Figure 1e. In theory, the wavelength dependence of the FL cross section (proportional to $1/\lambda^3$) is not the same as that of the SE cross section (proportional to $1/\lambda$). Therefore, the shape of FL and SE bands should not be perfectly coincident. In particular, because of such different wavelength dependencies, the SE band is expected to peak at lower energies, or longer wavelengths, as observed here. Anyway, we stress that within the spectral range of SE, and especially close to the ~565 nm peak, the gCDs may have enough optical gain for lasing under suitable pumping conditions.

In general, the optical response of CDs is very dependent on the specific structure and synthesis pathway. Indeed, the distinct optical gain characteristics of the carbon nitride dots used in this work are not common for CDs and make them especially suitable for laser[37] or random laser applications, as we aim to achieve in this study. Other minor contributions due to ground state bleaching and excited-state absorption can be recognized in the TA spectra of Figure 2a[47] and are not further discussed here.

Thereafter, we determined the value g of the amplification gain coefficient of gCDs by using the variable strip length (VSL) technique.[61,62] In the VSL method, the sample is excited by a strip-shaped beam of variable length l (Figure 2b). Measuring the intensity emitted from the edge of the sample,[62] $I(l) = [\exp(gl) - 1]$, then allows to estimate the gain coefficient g. We conducted VSL by hosting the gCDs inside a 10 mm square cuvette pumped by 435 nm pulses with a 2.30 mJ/mm^2 intensity. Figure 2c,d shows the observed behavior of $I(l)$, from which we extract g at two different concentrations: 4.60 ± 0.10 (gCD1 = 2g/L) and 13.0 ± 0.5 cm^{-1} (gCD2 = 4 g/L). For comparison, we repeated the same experiment for fluorescein dye under the same experimental conditions (that

https://doi.org/10.1021/acsphotonics.4c00279
ACS Photonics XXXX, XXX, XXX−XXX

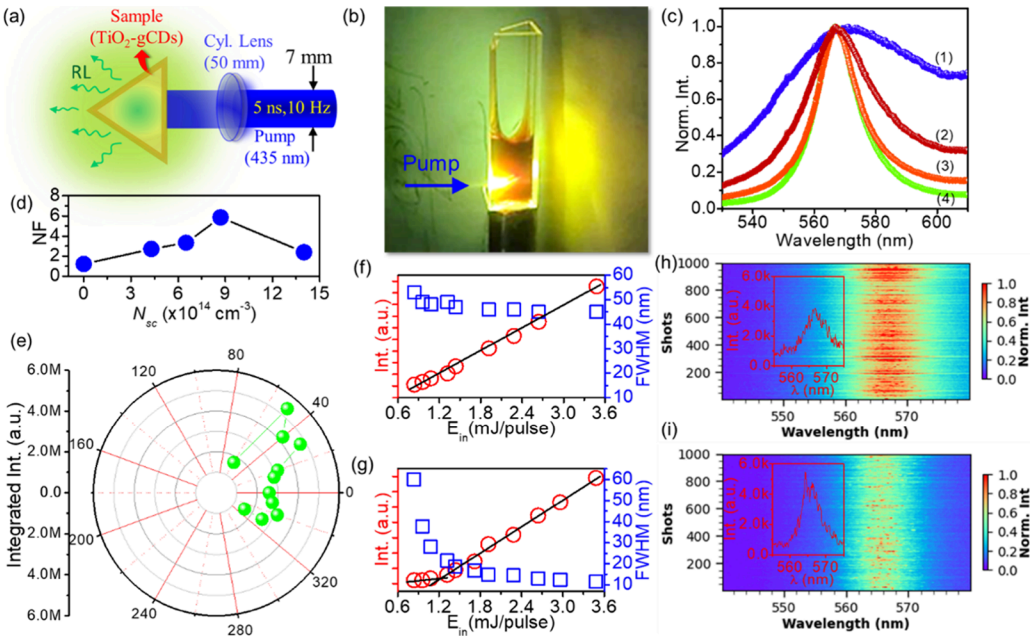

Figure 3. RL emission from gCDs in the presence of TiO_2 nanoparticles as passive scatterer. (a) Schematic of the experimental set up for detecting RL emission. (b) Digital photograph of the as designed RL system in operating conditions. (c) Normalized emission spectra (averaged over 1000 pump shots) under pumping with 435 nm pulses with 3.50 mJ energy of (1) bare gCD1 (~2 g/L concentration) and gCD1 in the presence of added TiO_2 in variable concentrations: $N_{sc} \approx$ (2) 4.30×10,[14] (3) 6.50×10,[14] and (4) 8.70×10^{14} cm^{-3}. (d) Variation of the narrowing factor with N_{sc}. (e) Angular distribution of the RL emission intensity. (f) Input vs output characteristics of bare gCD1 (~2 g/L) and (g) gCD1 with TiO_2 ($N_{sc} \approx 8.70 \times 10^{14}$ cm^{-3}). (h), (i): 2D color map of (h) gCD1 (~2 g/L) and (i) gCD2 (~4 g/L) in the presence of TiO_2 ($N_{sc} \approx 8.70 \times 10^{14}$ cm^{-3}), pumped at 435 nm (3.50 mJ/pulse), collecting 1000 consecutive single-shot emission spectra captured with high spectral resolution (0.15 nm).

is, the same peak absorption coefficient, as shown in Figure S2b) and pumping at peak absorption wavelength. Notably, the obtained value of g (8.5 ± 0.6 cm^{-1}, Figure S2c) for fluorescein is found to be less than gCD2. Moreover, the recorded values of g for the gCDs are higher than previously reported CDs.[33,63] In summary, such high values of σ_{em} and g, together with a well-defined gain spectral region as found from TA measurements, strongly suggest the possibility of achieving lasing by using gCDs in a wide concentration range.

Incoherent and Coherent Random Laser Emission from gCDs. On this ground, we demonstrated RL emission from a disordered system containing gCDs (gain media) and TiO_2 nanoparticles (34 nm diameter) serving as scatterers. The geometries of the experiments are schematically shown in Figure 3a. Spectral behavior of bare gCD1 and bare gCD1 in the presence of different concentrations of scatterers (N_{sc}) is shown in Figure 3c, reporting typical spectra collected under pulsed (5 ns) high power ($E_{in} \approx 3.50$ mJ/pulse) excitation at 435 nm.

While the emission of bare gCDs is quite similar to the spectrum recorded under low excitation intensity (Figure 1e), a clear spectral narrowing of the RL emission is observed with increasing N_{sc}. We can quantify the effect by a spectral narrowing factor, that is, the ratio fwhm (E_{in} = 0.15 mJ/pulse)/fwhm (E_{in} = 3.50 mJ/pulse) between the spectral widths recorded upon pumping below and above the threshold pump energy for spectral narrowing. As reported in Figure 3d, we observed an NF that increases with N_{sc} to a maximum of ~6, before ultimately decreasing again due to the detrimental influence of TiO_2 on CD emission at very high concentration. The spectral narrowing of CD emission induced by scatterers is a clear proof of RL emission promoted by multiple scattering events in the TiO_2-gCD system.[64]

Indeed, demonstration of narrowband laser emission from CDs hosted inside a resonator, or even simply contained in a square quartz cuvette, is now well-established in the literature.[46,65,66] However, reports of RL remain rare, and in some of them, it is not clear whether the narrowband emission is due to the optical feedback provided by the disordered active medium, which is the definition of RL, or at least partly due to the external feedback from the external cavity or cuvette parallel walls.[38,43] Also here, a strong unidirectional narrowband emission can be observed when gCDs (without added TiO_2) are kept inside a 1 cm square cuvette (Figure S3a), which works as a Fabry–Perot cavity. However, such a defined "beam" almost completely disappears when the lasing experiment is carried out if gCDs are inside a triangular cuvette (Figure S3b). In these conditions, the angular distribution of the RL emission generated from the TiO_2-gCD ($N_{sc} \approx 8.70 \times 10^{14}$ cm^{-3}) system is found to be broad (Figure 3e), which is very different from Fabry–Perot or other type of external feedback-assisted lasing.[67,68] Moreover, the wavelength and fwhm of the RL emission remain constant over a broad range of detection angles (inset, Figure S4a). This is a typical feature of RL deriving from the randomization effect of the optical path of both emitted and pump photons inside the gain medium, as produced by the effect of repeated scattering events.[69] Indeed, the use of triangular cuvettes is still insufficient to completely isolate RL. In fact, for strong pumping, one can still observe a weak directional beam caused by amplified stimulated emission (ASE), which leaves the cuvette within a small aperture cone along the pump strip direction (angle θ = 0), and coexists with the RL emission,

https://doi.org/10.1021/acsphotonics.4c00279
ACS Photonics XXXX, XXX, XXX−XXX

which is simultaneously emitted from the same system in all other directions. To conclusively differentiate this residual ASE from RL, we can resort to one key statistical properties of RL emission, which is the phenomenon called replica symmetry breaking (RSB), a statistical fingerprint of emission, which is not expected for "ordinary" lasing[70] and ASE.[71] Shortly, the onset of RSB can be highlighted by the change of shape of a statistical distribution function $P(q)$ of the so-called order parameter q, closely related to the pulse-to-pulse intensity correlation. In Figure S5, we have conducted an RSB analysis on a data set obtained by recording 500 (= N_{ps}) single shot emission spectra at pump energy $E_{in} \approx 2.30$ mJ/pulses ($>E_{in}^{Th}$), in two different directions: (i) the pump strip direction ($\theta = 0$, panel a), where we might expect some ASE, and (ii) a direction which is not along the pump strip ($\theta = 45°$, panel b). The shape of $P(q)$ is different in the two cases. Only at $\theta = 45°$ (or any other direction sufficiently far from $\theta = 0$) we see the typical two-peaked form of the $P(q)$ function, with maxima at the extremes, which is the unmistakable trademark of RL. In contrast, no RSB behavior is observed instead (panel a) when detecting at zero angle, because the light collected here stems, at least in part, from ASE. Because of this, all our RL experiments, such as those in Figure 3, were conducted in a triangular cuvette in order to avoid any Fabry−Perot response of the cavity and thus isolate the occurrence of true RL. Also, analysis of the emitted light was always conducted at $\theta > 10°$ to avoid any influence of residual ASE background.

Emission spectra of the bare gCDs and TiO_2-gCD colloidal mixtures ($N_{sc} \approx 8.70 \times 10^{14}$ cm^{-3}) at different E_{in} values are directly compared in Figure S4b,c (Supporting Information), while the quantitative dependence of emitted intensity and fwhm as a function of pumping energy for both systems is reported on Figure 3f,g. Figure 3f and Figure S4b show that for bare gCDs, we do not see substantial spectral narrowing with increase in E_{in}, and no clear inflection point is observed when the emission intensity is plotted vs E_{in}. On the other hand, Figure S4 reports the emission profiles of TiO_2-gCD1 ($N_{sc} \approx 8.70 \times 10^{14}$ cm^{-3}) as recorded at different E_{in} values. In this case, the progressive appearance of the sharp RL peak at ∼565 nm is obvious with an increasing pumping power. By analyzing these data, two key characteristics of RL emission[4] are clearly identifiable from Figure 3g: the change of slope in the dependence of the emission intensity with E_{in} and the onset of spectral narrowing both observed after a threshold pumping energy E_{in}^{Th} of ∼1.20 mJ/pulse. Above the threshold, the emission fwhm is reduced sharply from ∼60 to 10 nm, and the spectral position (560 nm) of narrow RL emission matches very well the stimulated emission peak recorded by TA data (Figure 2a), where the laser amplification is expected to be optimal. In regard to stability, we measured single-shot emission spectra of the TiO_2-gCD system pumped at $E_{in} \approx$ 1.90 mJ/pulses, for ∼10000 consecutive pump shots (2D color map in Figure S6a). Clearly, the spectral shape and intensity of the RL emission are both maintained throughout a large number of shots, indicating the optical and photochemical stability of the TiO_2-gCD system under continuous illumination. Moreover, the line shape of the RL emission is found almost unaltered even after 90 days from the preparation of colloidal TiO_2-gCD1 (Figure S6b). In summary, the evidence presented in Figure 3 clearly shows the possibility of using gCDs as a gain medium for stable RL in the presence of a suitable concentration of passive TiO_2 scatterers. On these grounds, we continued our study with the goal of achieving a full characterization of the fundamental properties of RL light emitted by the TiO_2-gCD RL source and, in particular, disentangling contributions due to coherent and incoherent RL.

One key aspect of random lasing is the existence of a large number of competing lasing modes, casually determined by the random arrangement of scatterers inside the gain medium and characterized by varying degrees of spatial localization.[72] In our case, the number of modes can be roughly estimated as $N_m = 2\pi A/l_p^2 \approx 10^6$, where $A \approx 1.5$ mm^2 and $l_p \approx 565$ nm are the excitation area and central wavelength, respectively.[73] The available photon modes change from shot to shot due to the spatial diffusion of the scatterers and, in a single shot, only a few longest lifetime modes will effectively contribute to lasing, as their gain is large enough for effective amplification.[74] As discussed in the introduction, RL can be classified as coherent of incoherent. The most common picture of coherent RL is that this is achieved when light gets effectively trapped by a strongly localized mode behaving as a looplike laser resonator. Its primary signature is the appearance of ultranarrow lasing spikes over a broader RL line shape. Because of spatial diffusion of the scatterers in time, this kind of coherence property of our CD-based random lasers can only be checked by recording single-shot RL spectra with sufficiently high resolution. To this purpose, we report in Figure S7 a sequence of 200 single-shot emission spectra by TiO_2-gCD mixtures for fixed scatterer concentration ($N_{sc} \approx 8.70 \times 10^{14}$ cm^{-3}) but two different CD concentrations (gCD1 = 2 g/L, gCD2 = 4 g/L). These spectra were collected by a high-resolution spectrometer with a resolution of ∼0.15 nm. From the spectra, it is obvious that narrow spikes with fwhm ∼0.7 nm, which are the fingerprint of coherent RL, randomly appear at some spectral positions over the comparatively broader (fwhm ≈ 10 nm) incoherent RL emission already discussed so far. As expected, the spikes randomly appear and disappear from shot to shot due to the random spatial fluctuations of the scatterers. Most interestingly, coherent spikes are only observed for higher CD concentration i.e., gCD2 (4 g/L), as reported in Figure S7b, while almost no coherent RL is produced by sample gCD1 (Figure S7a) where the concentration of CDs (2 g/L) is lower. Single shot RL emission profiles of TiO_2-gCD1 and TiO_2-gCD2 are also reported as color maps in Figure 3h,i, respectively. While coherent spikes can be noticed as bright spots in individual spectra in Figure 3i, the coherent contribution to RL is almost completely lost when averaging 100 single-shot spectra, as shown in the inset. Notably, average peak position of the RL emission for both TiO_2-gCD1 and TiO_2-gCD2 systems is found to be unchanged with gCD concentration as can be seen from Figure S8. Normally, a transition of incoherent to coherent RL emission is expected in the presence of high enough concentration of scatterers.[75−78] Our data show that coherent RL can actually be activated by an increase of CD concentration (Figure S7), thus increasing the concentration of the active chromophores. This may happen due to either additional scattering provided by the gCDs or reduction in the gain length, which is a consequence of the increase of gain g when going from gCD1 to gCD2 (Figure 2). Therefore, owing to the smaller l_g, inside an effective loop gain can be achieved easily for the TiO_2-gCD2 system by overcoming the loss,[79,80] and RL emission due to the coherent feedback is observed. As an alternative, we also tried to achieve coherent RL by increasing the concentration of TiO_2 scatterers, when keeping a fixed concentration of CDs.

https://doi.org/10.1021/acsphotonics.4c00279
ACS Photonics XXXX, XXX, XXX−XXX

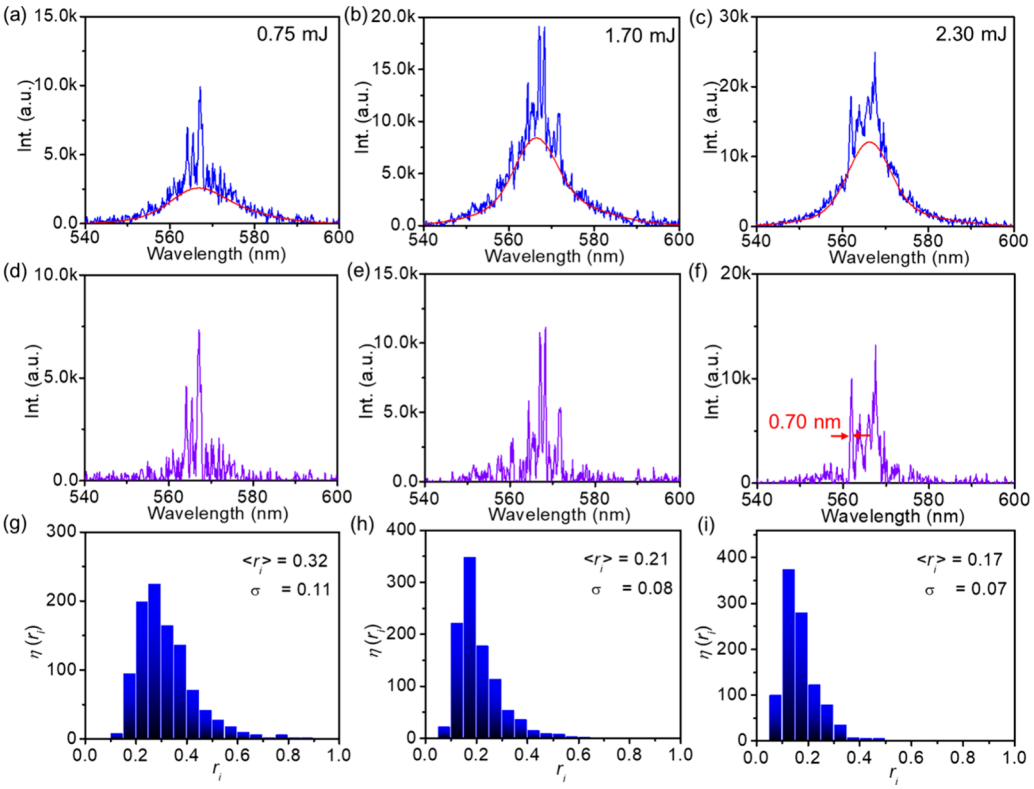

Figure 4. Statistical analysis of the incoherent and coherent RL emission. Emission spectra of the TiO_2-gCD2 ($N_{sc} \approx 8.70 \times 10^{14}$ cm^{-3}) RL along with their incoherent part (shown in red) collected at an E_{in} values of (a) ~0.75, (b) 1.70, and (c) 2.30 mJ/pulses. (d–f) Coherent parts obtained after subtracting the incoherent part from the total emission and (g–i) the probability distributions of coherent-to-incoherent ratios, corresponding to the spectra shown in (a–c), respectively. $\langle r_i \rangle$ and σ are the mean value and standard deviation of the probability distribution function $\eta(r_i)$, respectively.

However, this strategy turned out to be ineffective. In fact, at higher TiO_2 concentrations the systems fails to generate the coherent RL modes (Figure S9b,d) and a certain broadening of RL emission is observed (not shown). Also, it may be due to the effect of collisional quenching or photoelectron charge transfer, which still needs to be studied yet. Thereafter, we have tried to precisely pinpoint the concentration threshold of gCDs at which the transition from incoherent to coherent RL emission takes place. To do this, we have performed the RL experiment at different concentration of gCDs ranging from ~1 to 8 g/L with a fixed amount of scatterers (TiO_2, $N_{sc} \approx 8.70 \times 10^{14}$ cm^{-3}). In this respect, it is worth noting that the concentration range that can be explored is practically limited by solubility (on the higher end) and by the need of achieving sufficient laser gain (on the lower end). The pump energy-dependent RL emission spectra for each of the combinations are shown in Figure S10a–f. For each of the cases, spectral narrowing is observed at sufficiently high pump intensity E_{in} (inset of Figure S10). Also, E_{in}^{Th} for the incoherent RL emission is observed to be decreasing from ~1.43 to 0.71 mJ/pulses with an increase in the concentration of gCD from ~1 to 8 g/L (Figure S11a–f). Single-shot RL emission profiles collected at E_{in} = 1.70 mJ/pulses for each of the TiO_2-gCD systems are shown in the 2D color maps shown in inset (i) of Figure S11a–f, together with individual typical spectra, plotted in inset (ii) of Figures S11a–f. These data clearly allow identification of the experimental conditions where coherent RL occurs: at the highest explored concentrations (~3 to 8 g/L), the appearance of low coherent RL emission over a consistent incoherent background can be readily identified from both the bright isolated spots in the 2D color map and the narrow spikes in the typical exemplary spectra. Both these spots and narrow spikes are only observed at gCD concentrations ~3g/L and higher, while they are absent at ~1 and 2 g/L. Therefore, these data clearly pinpoint the transition between incoherent and coherent RL to occur between gCD concentrations of ~2 and 3 g/L.

Considering that RL results from laser amplification occurring along random paths controlled by the random diffusion of the scatterers over time (in a liquid medium), the spectral position of the coherent modes changes from one laser shot to the next. Therefore, it is not possible to observe coherent modes by averaging many shots, as one would be tempted to do to increase the signal-to-noise ratio of the measurements. In contrast, to analyze the characteristics of RL, as for example the ratio between coherent and incoherent RL contributions, it is necessary to resort to a shot-to-shot statistical analysis such as proposed in Figure 4. To this purpose, for each single-shot emission spectrum, we subtracted the broad incoherent profile obtained by interpolating the local minima of the coherent spikes, as shown in Figure 4a–c, to isolate the coherent contributions (Figure 4d–f). The fraction of coherent to incoherent intensity for each spectrum in the sequence (i = 1···1000) can be defined as $\langle r_i \rangle = \langle I_c \rangle_\lambda / \langle I_{ic} \rangle_\lambda$, where $\langle I_c \rangle_\lambda$ and $\langle I_{ic} \rangle_\lambda$ are the wavelength-averaged (spectral range: 560–575 nm) coherent and incoherent intensities of the RL emission profile. On these grounds, we plot in Figure 4g–i the probability distribution of the quantity $\langle r_i \rangle$, i.e., $\eta(r_i)$, corresponding to three pumping intensities of sample TiO_2-gCD2. The results corresponding to the data shown in Figure

https://doi.org/10.1021/acsphotonics.4c00279
ACS Photonics XXXX, XXX, XXX–XXX

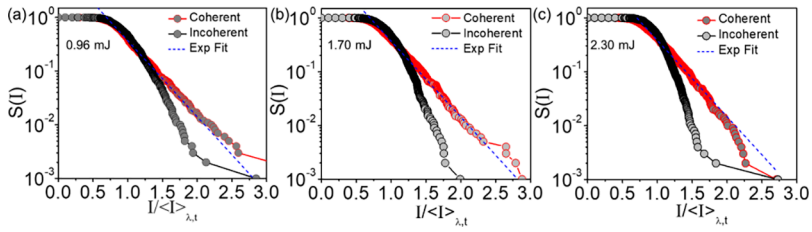

Figure 5. Decay behavior of the survival functions. Survival functions $S_{inc}(I)$ and $S_{coh}(I)$, of the incoherent and coherent components, respectively, of the TiO_2-gCD2 RL emission at three pump energies: (a) 0.96, (b) 1.70, and (c) 2.30 mJ/pulses. The exponential decay profile is indicated by a blue dashed line.

4a–c are presented in Figure 4g–i, respectively. When the system is pumped at low $E_{in} \approx 0.75$ mJ/pulse (Figure 4g), corresponding to the laser threshold for TiO_2-gCD2 (Figure S11c), the value of $\langle r_i \rangle$ is determined to be 0.32. This means that ~32% of the emitted RL intensity is attributed to the coherent spikes. Subsequently, as the pump intensity E_{in} increases, the value of $\langle r_i \rangle$ decreases, reaching $\langle r_i \rangle \geq 0.17$ at $E_{in} \approx 2.30$ mJ/pulse (Figure 4i). A similar statistical analysis is also done for the TiO_2-gCD2 system at three different N_{sc} values ranging from ~4.30 to 8.70×10^{14} cm^{-3}, as shown in Figure S12. Notably, $\eta(r_i)$, is found to increase when increasing the concentration of TiO_2 from ~4.30×10^{14} cm^{-3}, where coherent RL is barely appreciable, to ~8.70×10^{14} cm^{-3}, where strong coherent spikes appear over the incoherent RL background. With further increases of TiO_2 concentration, we observe a sudden drop in RL efficiency (see Figure 3d), most likely due to quenching of CD emission due to charge transfer to TiO_2, and no coherent RL is observed anymore.

Generally speaking, the statistical properties of random lasers are the subject of undergoing theoretical discussion in the literature and still not fully understood.[19,75,81] Anyway, the observed behavior of $\langle r_i \rangle$ appears to be characteristic of RLs displaying both incoherent and coherent output,[19] and a tentative explanation for it was provided in a previous work:[10] as spectral self-averaging due to the increase in the number of coherent modes occurs above a critical E_{in}, the incoherent contribution becomes more and more dominant over the coherent one at higher E_{in}.

Furthermore, we have analyzed the so-called survival function $S(I)$ of the intensity, another quantity of significant theoretical interest[82] which provides an additional route to recognize the individual contributions of coherent and incoherent RL. Generally, the emission probability of RL modes at a particular intensity I can be described by $S(I)$,[82] which is defined as the fraction of shots with emission intensity larger than I. Here, the $S(I)$ have been evaluated by following the method reported in earlier studies on dye-based optofluidic RLs.[19,75]

In brief, intensity of the incoherent and coherent component of the TiO_2-gCD2 RL emission are extracted as in Figure 4 and separately normalized by their corresponding wavelength- and shot- averaged values. Thereafter, one numerically estimates the quantities $S(I,\lambda)$ at each wavelength, and finally averages over wavelengths (560 to 575 nm) to obtain two $S(I)$ functions corresponding to the incoherent and coherent parts of the RL emission, respectively. In Figure 5, we show the $S(I)$ of incoherent and coherent intensity components as observed for three different pumping intensities E_{in}. In all cases, the decay behavior of the $S_{inc}(I)$ corresponding to the incoherent RL component is found to be faster than an exponential decay profile. In contrast, $S_{coh}(I)$ of the coherent part displays an approximately exponential decay tail, which significantly extends toward higher intensity values. This behavior is observed at all pumping energies above the E_{in}^{Th} of ~0.75 mJ/pulses, although it seems to become less clear at the highest pumping energies (Figure 5c), likely due to the increasingly dominant contribution of incoherent part and the onset of gain saturation.

The long tail of the $S_{coh}(I)$ survival function for coherent RL, as compared to the faster decay of the incoherent $S_{inc}(I)$, have been pinpointed as characteristic features discriminating the statistical properties of the two types of RL.[19,82] The slower-than-exponential decay of $S_{inc}(I)$ can be attributed to the onset of gain saturation,[19] limiting the probability of high-intensity RL shots in the incoherent case, more than it does for coherent RL. In general, the slow-decaying tail of $S_{coh}(I)$ can display different functional forms ranging from power law to exponential, in the context of an ongoing theoretical discussions.[19,75,81] The exponential form was already observed in dye-based systems and tentatively attributed to the generation of amplified long-path extended modes, capable of large amplification and ultranarrow coherent emission, rather than truly, Anderson-type localized modes that are most commonly associated with coherent RL.[10,11,19] Indeed, a strong localization of photons inside a disorder system can be achieved when the transport mean free path (l_t) of light becomes comparable to wavelength.[83,84] In our case, l_t at 565 nm can be estimated to be of the order of millimeters, from the extinction spectra recorded from an aqueous suspension of TiO_2 nanoparticles (see Figure S13 and related discussion). Therefore, no strong light localization is possible here, further supporting the generation of amplified long-path extended modes as the most likely mechanism by which coherent RL is obtained in our system, as suggested by the form of the $S_{coh}(I)$ survival function. While more studies will be needed to fully clarify the statistical properties of CD-based RL emission, the present analysis is certainly consistent with our attributions of their RL output as a combination of coherent and incoherent contributions with variable relative weights based on pumping intensity E_{in} (Figure 4) and CD concentration (Figure 3h–i and Figure S7). Importantly, we have shown that by controlling these two parameters, we have the opportunity to generate both the coherent and incoherent RL emission for customized application using a single colloidal disorder system such as TiO_2-gCD2.

A few recent works in the literature have pioneered the field by observing narrowband emission from carbon dots with clear contributions due to coherent RL, as can be inferred from the observation of ultranarrow peaks on a broader background.[41,65,66] However, we stress here that only the statistical analysis of the emission at the single-shot level at the single-shot, as shown in Figures 4 and 5, together with studies in

https://doi.org/10.1021/acsphotonics.4c00279
ACS Photonics XXXX, XXX, XXX–XXX

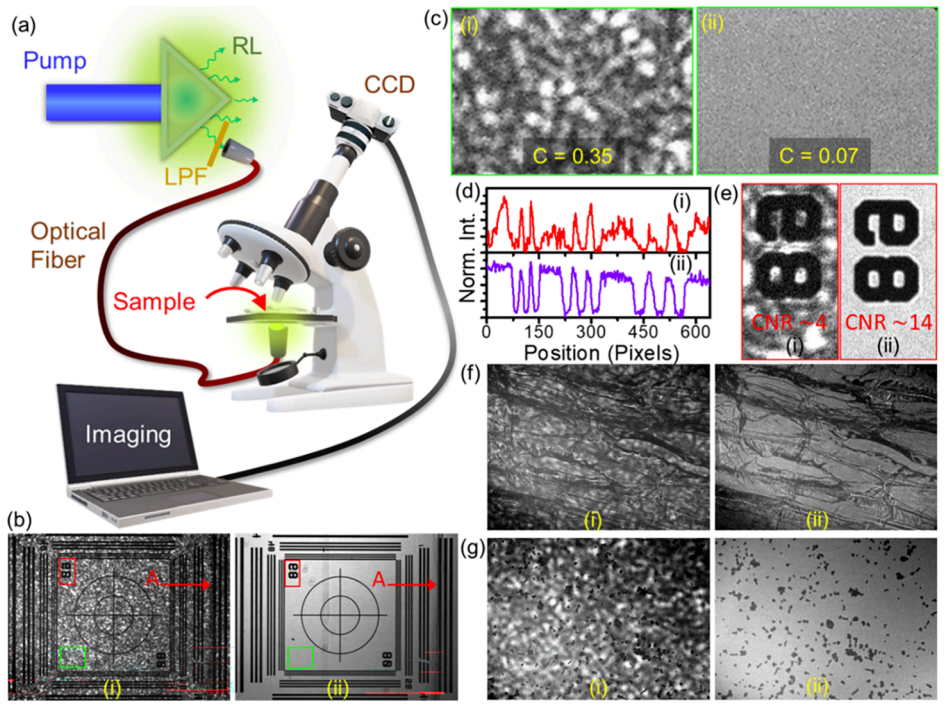

Figure 6. gCD-based RL emission as a source for speckle free microscopy. (a) Experimental setup for speckle free imaging using TiO_2-gCD2 RL ($N_{sc} = 8.70 \times 10^{14}$ cm^{-3}) as the illumination source. (b) Images of the NBS 1952 resolution test target under the illumination from (i) 405 nm diode laser and (ii) TiO_2-gCD2 RL. (c) Enlarged version of green rectangular zone, as indicated in (b), used for estimation of the speckle contrast *C*. (d) Intensity distribution of the features of the resolution test target along the line "A" as indicated in (b). (e) Enlarged version of red rectangular zone as indicated in (b), used to estimate the contrast to noise ratio (CNR). Images of the (f) *Allium cepa* cell membrane and (g) polystyrene microparticles (~3 μm) imaged under the illumination of (i) 405 nm diode laser and (II) TiO_2-gCD2 RL.

different geometries (Figure S3 vs Figure 3) and in the presence of variable concentrations of carbon dots (Figures S10 and S11) and external scatterers (Figure 3, Figures S9 and S12) allows conclusively discriminate the several possible contributions (amplified stimulated emission, Fabry−Perot lasing, coherent and incoherent RL) to the overall narrowband emission and pinpoint the precise origin of the RL phenomenon. In addition, the present data also allow to clearly identify, for the first time, the conditions capable of triggering a transition from incoherent to coherent RL.

Speckle-Free Imaging Microscopy Using the GCD-Based RL as Light Source. From a practical point of view, both coherent and incoherent RL emissions have several applications. For instance, coherent RL has been used for the generation of optical bits, barcode, and encryption.[14,15] All types of RL are advantageous light sources for speckle-free imaging, because of the low spatial coherence of RL emission.[3,18] In the following, we demonstrate the proof-of-concept use of our CD-based RL in speckle-free imaging under a conventional microscope setup.

Our setup for speckle free imaging experiments is schematically shown in Figure 6a and described in detail in the Experimental Section. Two kinds of sources were used for illumination inside a microscope: (i) a commercial 405 nm laser diode and (ii) the RL emission peaking at ~565 nm generated from the colloidal TiO_2-gCD2 at $E_{in} \approx 3.50$ mJ/ pulses. Initially, we used a NBS 1952 resolution test target (Thorlabs, R1L3S10P) as the imaged object.

Unlike conventional laser illumination, a clear speckle free image of the imaged object is obtained when it is illuminated under the RL (Figure 6b). In contrast, the image illuminated by the traditional laser diode, which is a highly coherent source, produces a speckle corrupted noisy image. The so-called speckle contrast $C = \rho/\bar{I}$, where ρ is the standard deviation of the image intensity and $\bar{I}$ is the average intensity of the image, can be used as a tool to analyze the degree of spatial coherence.[85] Ideally, $C = 1$ corresponds to very high spatial coherency, whereas $C = 0$ is fully incoherent. In our case, the green rectangular zone in Figure 6b has been used to determine the value of *C*. Clearly, as can be seen from Figure 6c, the value *C* is found to be ~0.07 for the RL illumination, which is 5 times less than the *C* value for laser diode illumination. Additionally, features of the imaged object as inspected along line "A" are clearly distinguishable when the image has been captured under RL illumination (Figure 6c). Finally, a quantitative comparison of image quality has been done after estimating the contrast-to-noise ratio, defined as $CNR = (\bar{I}_f - \bar{I}_b)/((\rho_f + \rho_b)/2)$[18,45] where $\bar{I}_f$ is the average intensity of the feature of interest (a portion of the number "8" in Figure 6e), $\bar{I}_b$ is the average intensity of the surrounding background, and ρ_f (ρ_b) is the standard deviation of pixel intensity of the feature of interest, i.e., the background. Here, we have taken the red rectangular zone of the image shown in Figure 6b to determine CNR. Generally, under an illumination with high spatial coherence, the feature of interest in an imaging object can be hard to distinguish from noise, and the CNR approaches 1. As demonstrated in Figure 6e, the CNR for the image is significantly higher (~14) under the illumination of the TiO_2-gCD2 RL due to its low spatial coherence. The *C* and CNR here reported are quite similar or even better than the previously data reported for other RL emissions.[86,87]

When repeating these experiments at different CD concentrations, we found that the characteristic of the captured

https://doi.org/10.1021/acsphotonics.4c00279
ACS Photonics XXXX, XXX, XXX−XXX

images does not differ significantly when TiO2-gCD1 and TiO2-gCD2 RL systems are used as the source of illumination. Indeed, as discussed in the previous section, the relative weight of the coherent RL contribution quickly decreases with higher excitation power. As the speckle-free imaging experiments were done at relatively high pump energy of ∼3.50 mJ/pulses (compare with Figure 4), the incoherent portion of RL is always dominant, such that the CD concentration used in the RL light source is practically irrelevant to the purposes of these speckle-free imaging experiments.

Anyway, the as designed CD-based RL source can be potentially used as an illuminating source for microscopy, as we further demonstrate by imaging a biological tissue such as *Allium cepa* cell membrane (Figure 6f) or a collection of polystyrene microparticles over a glass slide (Figure 6g). Image quality is quite clear for both of these imaged objects under the RL illumination.

CONCLUSIONS

In summary, β-C_3N_4 type gCDs with distinct stimulated emission can be used as gain media for the generation of RL emission in the presence of TiO_2 nanoparticles. In suitable experimental conditions, the colloidal disordered system containing gCDs emits RL emission at ∼565 nm, with an wide angular distribution and ∼10 nm line width, corresponding to a narrowing factor of ∼6 from CD fluorescence. Increasing the concentration of gCDs above a certain threshold causes a transition from incoherent to coherent RL emission, which is demonstrated by the appearance of ultranarrow emission peaks (∼0.7 nm) with spectral positions fluctuating from shot to shot. A detailed statistical analysis of coherent RL emission allows to tentatively attribute it to the formation of amplified extended modes with exceptionally high gain. Finally, the low spatial coherence of the gCD based RL is exploited for high performance speckle free imaging of different test objects. Overall, the as designed TiO_2-gCD RL can be used as a biocompatible low cost light source for high contrast imaging of biological tissues, surfaces, and inorganic microstructures.

ASSOCIATED CONTENT

Supporting Information

The Supporting Information is available free of charge at https://pubs.acs.org/doi/10.1021/acsphotonics.4c00279.

Concentration dependent optical properties of gCDs; steady state and time-dependent optical properties of gCD1, gCD2 and fluorescein dye for comparison; emission characteristics of bare gCDs hosted inside quartz cuvettes of different shapes; angle- and pump energy-dependent emission spectra of gCD-based colloidal disorder systems; stability of colloidal TiO_2-gCD1 RL; effect of concentration of gCDs on RL emission wavelength; high-resolution single shot emission spectra gCD based RL systems; effect of N_{sc}, and concentration of gCDs on spectral features of gCD-based RL systems; statistical analysis of the incoherent and coherent RL emission for different N_{sc} values of TiO_2; incoherent RL emission characteristics of the colloidal TiO_2-gCD2 RL; and experimental determination of the transport mean free path (l_t) (PDF)

AUTHOR INFORMATION

Corresponding Author

Fabrizio Messina − *Dipartimento di Fisica e Chimica "Emilio Segrè" and ATeN Center, Università degli Studi di Palermo, Palermo 90123, Italy;* orcid.org/0000-0002-2130-0120; Email: fabrizio.messina@unipa.it

Authors

Ashim Pramanik − *Dipartimento di Fisica e Chimica "Emilio Segrè", Università degli Studi di Palermo, Palermo 90123, Italy*

Marco Reale − *Dipartimento di Fisica e Chimica "Emilio Segrè", Università degli Studi di Palermo, Palermo 90123, Italy*

Marco Cannas − *Dipartimento di Fisica e Chimica "Emilio Segrè", Università degli Studi di Palermo, Palermo 90123, Italy;* orcid.org/0000-0001-8236-5043

Radian Popescu − *Laboratory for Electron Microscopy, Karlsruhe Institute of Technology, Karlsruhe 76131, Germany*

Alice Sciortino − *Dipartimento di Fisica e Chimica "Emilio Segrè" and ATeN Center, Università degli Studi di Palermo, Palermo 90123, Italy;* orcid.org/0000-0001-8361-3002

Complete contact information is available at: https://pubs.acs.org/10.1021/acsphotonics.4c00279

Author Contributions

The manuscript was written through the contributions of all authors. All authors have approved the final version of the manuscript.

Notes

The authors declare no competing financial interest.

ACKNOWLEDGMENTS

EU is acknowledged for financial support (CARLITO, Grant agreement ID: 101061538). A.S. acknowledges funding from Fondo Finalizzato Alla Ricerca Di Ateneo (FFR) 2022-2023 of UNIPA.

REFERENCES

(1) Zhang, J.; Wang, F.; Ghafoor, S.; Wang, H.; Zhang, W.; Xie, K.; Cheng, R.; Yan, J.; Niu, L.; Wang, P.; Zhang, L.; Hu, Z. Tunable Plasmonic Random Laser Based on Emitters Coupled to Plasmonic Resonant Nanocavities of Silver Nanorod Arrays. *Adv. Opt. Mater.* **2022**, *10*, 2200426.

(2) Redding, B.; Choma, M. A.; Cao, H. Spatial Coherence of Random Laser Emission. *Opt. Lett.* **2011**, *36*, 3404−3406.

(3) Zhan, Z.; Liu, Z.; Du, J.; Huang, S.; Li, Q.; Hu, Z.; Luo, J.; Yang, Y.; Dong, S.; Wang, L.; Tang, J.; Leng, Y. Thermally Evaporated $MAPbBr_3$ Perovskite Random Laser with Improved Speckle-Free Laser Imaging. *ACS Photonics* **2023**, *10*, 3077−3086.

(4) Luan, F.; Gu, B.; Gomes, A. S. L.; Yong, K. T.; Wen, S.; Prasad, P. N. Lasing in Nanocomposite Random Media. *Nano Today* **2015**, *10*, 168−192.

(5) Lawandy, N. M.; Balachandran, R. M.; Gomes, A. S. L.; Sauvain, E. Laser Action in Strongly Scattering Media. *Nature* **1994**, *368*, 436−438.

(6) Liang, S.; Yin, L.; Zhang, Z.; Xia, J.; Xie, K.; Zou, G.; Hu, Z.; Zhang, Q. Coherent Random Lasing Controlled by Brownian Motion of the Active Scatterer. *J. Phys. B* **2018**, *51*, 95401.

(7) Tolentino Dominguez, C.; Gomes, M. d. A.; Macedo, Z. S.; de Araújo, C. B.; Gomes, A. S. L. Multi-photon Excited Coherent Random Laser Emission in ZnO Powders. *Nanoscale* **2015**, *7*, 317−323.

(8) Consoli, A.; López, C. Decoupling gain and feedback in coherent random lasers: experiments and simulations. *Sci. Rep.* **2015**, *5*, 16848.
(9) Shi, X.; Wang, Y.; Wang, Z.; Wei, S.; Sun, Y.; Liu, D.; Zhou, J.; Zhang, Y.; Shi, J. Random Lasing with a High Quality Factor over the Whole Visible Range Based on Cascade Energy Transfer. *Adv. Opt. Mater.* **2014**, *2*, 88−93.
(10) Uppu, R.; Mujumdar, S. On the Coherent Modes of Ultranarrowband Random Lasers with Nonresonant Feedback. *Appl. Opt.* **2011**, *50*, E13−E19.
(11) Mujumdar, S.; Ricci, M.; Torre, R.; Wiersma, D. S. Amplified Extended Modes in Random Lasers. *Phys. Rev. Lett.* **2004**, *93*, 53903.
(12) Polson, R. C.; Vardeny, Z. V. Cancerous Tissue Mapping from Random Lasing Emission Spectra. *J. Opt.* **2010**, *12*, 24010.
(13) Wang, Y.; Duan, Z.; Qiu, Z.; Zhang, P.; Wu, J.; Zhang, D.; Xiang, T. Random Lasing in Human Tissues Embedded with Organic Dyes for Cancer Diagnosis. *Sci. Rep.* **2017**, *7*, 8385−8391.
(14) Li, J.; Liu, J.; Liu, D.; Tian, W.; Jin, S.; Hu, S.; Guo, J.; Jin, Y. Ultrafast Random Number Generation Based on Random Laser. *J. Light. Technol.* **2023**, *41*, 5233−5243.
(15) Sznitko, L.; Chtouki, T.; Sahraoui, B.; Mysliwiec, J. Bichromatic Laser Dye as a Photonic Random Number Generator. *ACS Photonics* **2021**, *8*, 1630−1638.
(16) Su, C. Y.; Hou, C. F.; Hsu, Y. T.; Lin, H. Y.; Liao, Y. M.; Lin, T. Y.; Chen, Y. F. Multifunctional Random-Laser Smart Inks. *ACS Appl. Mater. Interfaces* **2020**, *12*, 49122−49129.
(17) Zhang, Y.; Wang, S.; Zheng, C.; Zhang, W. Coherent Random Fiber Laser-Enabled Super-Resolution Spectroscopy. *ACS Photonics* **2023**, *10*, 2670−2678.
(18) Redding, B.; Choma, A. A.; Cao, H. Speckle-Free Laser Imaging Using Random Laser Illumination. *Nat. Photonics* **2012**, *6*, 355−359.
(19) Sarkar, A.; Bhaktha, B. N. S. Replica Symmetry Breaking in Coherent and Incoherent Random Lasing Modes. *Opt. Lett.* **2021**, *46*, 5169−5172.
(20) Uppu, R.; Tiwari, A. K.; Mujumdar, S. Identification of Statistical Regimes and Crossovers in Coherent Random Laser Emission. *Opt. Lett.* **2012**, *37*, 662−664.
(21) Gollner, C.; Ziegler, J.; Protesescu, L.; Dirin, D. N.; Lechner, R. T.; Fritz-Popovski, G.; Sytnyk, M.; Yakunin, S.; Rotter, S.; Yousefi Amin, A. A.; Vidal, C.; Hrelescu, C.; Klar, T. A.; Kovalenko, M. V.; Heiss, W. Random Lasing with Systematic Threshold Behavior in Films of CdSe/CdS Core/Thick-Shell Colloidal Quantum Dots. *ACS Nano* **2015**, *9*, 9792−9801.
(22) Wang, L.; Yang, M.; Zhang, S.; Niu, C.; Lv, Y. Perovskite Random Lasers, Process and Prospects. *Micromachines* **2022**, *13*, 2040.
(23) Jiang, X.; Zhao, X.; Bao, W.; Shi, R.; Zhao, J.; Kang, J.; Xia, X.; Chen, H.; Li, H.; Xu, J.; Zhang, H. Graphdiyne Nanosheets for Multicolor Random Lasers. *ACS Appl. Nano Mater.* **2020**, *6*, 4990−4996.
(24) Wang, J.; Zheng, J.; Yang, Y.; Liu, X.; Qiu, J.; Tian, Y. Tunable Full-Color Solid-State Fluorescent Carbon Dots for Light Emitting Diodes. *Carbon* **2022**, *190*, 22−31.
(25) Hola, K.; Sudolska, M.; Kalytchuk, S.; Nachtigallova, D.; Rogach, A. L.; Otyepka, M.; Zboril, R. Graphitic Nitrogen Triggers Red Fluorescence in Carbon Dots. *ACS Nano* **2017**, *11*, 12402−12410.
(26) Zhang, Y.; Wang, L.; Hu, Y.; Sui, L.; Cheng, L.; Lu, S. Centralized Excited States and Fast Radiation Transitions Reduce Laser Threshold in Carbon Dots. *Small* **2023**, *19*, 2207983.
(27) Wareing, T. C.; Gentile, P.; Phan, A. N. Biomass-Based Carbon Dots: Current Development and Future Perspectives. *ACS Nano* **2021**, *15*, 15471−15501.
(28) Pramanik, A.; Biswas, S.; Tiwary, C. S.; Kumbhakar, P.; Sarkar, R.; Kumbhakar, P. Forster Resonance Energy Transfer Assisted White Light Generation and Luminescence Tuning in a Colloidal Graphene Quantum Dot-Dye System. *J. Colloid Interface Sci.* **2020**, *565*, 326−336.
(29) Shi, Y.; Su, W.; Yuan, F.; Yuan, T.; Song, X.; Han, Y.; Wei, S.; Zhang, Y.; Li, Y.; Li, X.; Fan, L. Carbon Dots for Electroluminescent Light-Emitting Diodes: Recent Progress and Future Prospects. *Adv. Mater.* **2023**, *35*, 2210699.
(30) Chen, M.; Guan, L.; Ma, H.; Zhang, Y.; Chang, Y.; Wang, F.; Liu, Z.; Li, X. Spectral Regulation of Carbon Dots and the Realization of Single-Component Solar-Simulated White Light-Emitting Diodes. *ACS Photonics* **2023**, *10*, 2730−2738.
(31) Dong, X.-Y.; Niu, X.-Q.; Zhang, Z.-Y.; Wei, J.-S.; Xiong, H.-M. Red Fluorescent Carbon Dot Powder for Accurate Latent Fingerprint Identification Using an Artificial Intelligence Program. *ACS Appl. Mater. Interfaces* **2020**, *12*, 29549−29555.
(32) Lin, Z.; Yang, J.; Zeng, Q.; Tie, S.; Huang, R.; Lan, S. Deep Blue Photoluminescence and Optical Gain from Sodium-doped Carbon Dots. *J. Lumin.* **2022**, *246*, No. 118856.
(33) Zhang, W. F.; Tang, L. B.; Yu, S. F.; Lau, S. P. Observation of White-Light Amplified Spontaneous Emission from Carbon Nanodots under Laser Excitation. *Opt. Mater. Express* **2012**, *2*, 490−495.
(34) Leonetti, M.; Sapienza, R.; Ibisate, M.; Conti, C.; López, C. Optical gain in DNA-DCM for lasing in photonic materials. *Opt. Lett.* **2009**, *34*, 3764−3766.
(35) Bisschop, S.; Geiregat, P.; Aubert, T.; Hens, Z. The Impact of Core/Shell Sizes on the Optical Gain Characteristics of CdSe/CdS Quantum Dots. *ACS Nano* **2018**, *12*, 9011−9021.
(36) Alvarado-Leaños, A. L.; Cortecchia, D.; Folpini, G.; Srimath Kandada, A. R.; Petrozza, A. Optical Gain of Lead Halide Perovskites Measured via the Variable Stripe Length Method: What We Can Learn and How to Avoid Pitfalls. *Adv. Opt. Mater.* **2021**, *9*, 2001773.
(37) Sciortino, A.; Mauro, N.; Buscarino, G.; Sciortino, L.; Popescu, R.; Schneider, R.; Giammona, G.; Gerthsen, D.; Cannas, M.; Messina, F. β-C_3N_4 Nanocrystals: Carbon Dots with Extraordinary Morphological, Structural, and Optical Homogeneity. *Chem. Mater.* **2018**, *30*, 1695−1700.
(38) Zhu, H.; Zhang, W.; Yu, S. F. Realization of Lasing Emission from Graphene Quantum Dots using Titanium Dioxide Nanoparticles as Light Scatterers. *Nanoscale* **2013**, *5*, 1797−1802.
(39) Bharathi, D.; Krishna, R. H.; Siddlingeshwar, B.; Divakar, D. D.; Alkheraif, A. A. Understanding the Interaction of Carbon Quantum Dots with CuO and Cu_2O by Fluorescence Quenching. *J. Hazard. Mater.* **2019**, *369*, 17−24.
(40) Prajapati, R.; Bhattacharya, A.; Mukherjee, T. K. Resonant Excitation Energy Transfer from Carbon Dots to Different Sized Silver Nanoparticles. *Phys. Chem. Chem. Phys.* **2016**, *18*, 28911−28918.
(41) Yuan, F.; Xi, Z.; Shi, X.; Li, Y.; Li, X.; Wang, Z.; Fan, L.; Yang, S. Ultrastable and Low-Threshold Random Lasing from Narrow-Bandwidth-Emission Triangular Carbon Quantum Dots. *Adv. Opt. Mater.* **2019**, *7*, 1801202.
(42) Lyu, J.; Zhang, X.; Cai, L.; Tao, L.; Ma, W.; Li, A.; Tian, Y.; Yin, Y.; Kong, D.; Yi, W.; Wang, X.; Liu, R. Low-threshold and Narrow-emission Random Lasing in a Self-assembly TiN Nanoparticle-doped Carbon Quantum Dot/DCM Nanowire Composite. *Photonics Res.* **2022**, *10*, 2239−2246.
(43) Ni, Y.; Li, X.; Liang, W.; Zhang, S.; Xu, X.; Li, Z.; Li, L.; Shao, Y.; Ruan, S.; Zhang, W. Transformation of Random Lasing to Fabry−Perot Lasing: Observation of High Temperature Lasing from Carbon Dots. *Nanoscale* **2021**, *13*, 7566−7573.
(44) Zhang, M.; Dai, H.; Chen, X. Tunable Narrowband Carbon Quantum Dots Laser Based on Self-Assembled Microstructure. *Adv. Opt. Mater.* **2023**, *11*, 2301156.
(45) Zhang, Y.; Wang, J.; Wang, L.; Fu, R.; Sui, L.; Song, H.; Hu, Y.; Lu, S. Carbon Dots with Blue-to-Near-Infrared Lasing for Colorful Speckle-Free Laser Imaging and Dynamical Holographic Display. *Adv. Mater.* **2023**, *35*, 2302536.
(46) Messina, F.; Sciortino, L.; Popescu, R.; Venezia, A. M.; Sciortino, A.; Buscarino, G.; Agnello, S.; Schneider, R.; Gerthsen, D.; Cannas, M.; Gelardi, F. M. Fluorescent Nitrogen-rich Carbon Nanodots with an Unexpected β-C_3N_4 Nanocrystalline Structure. *J. Mater. Chem. C* **2016**, *4*, 2598−2605.
(47) Sciortino, A.; Madonia, A.; Gazzetto, M.; Sciortino, L.; Rohwer, E. J.; Feurer, T.; Gelardi, F. M.; Cannas, M.; Cannizzo, A.; Messina, F.

https://doi.org/10.1021/acsphotonics.4c00279
ACS Photonics XXXX, XXX, XXX−XXX

The Interaction of Photoexcited Carbon Nanodots with Metal Ions Disclosed down to the Femtosecond Scale. *Nanoscale* **2017**, *9*, 11902−11911.
(48) Guo, L.; Ge, J.; Liu, W.; Niu, G.; Jia, Q.; Wang, H.; Wang, P. Tunable Multicolor Carbon Dots Prepared from Well-Defined Polythiophene Derivatives and Their Emission Mechanism. *Nanoscale* **2016**, *8*, 729−734.
(49) Zulfajri, M.; Sudewi, S.; Damayanti, R.; Huang, G. G. Rambutan Seed Waste-derived Nitrogen-doped Carbon Dots with L-aspartic Acid for the Sensing of Congo Red Dye. *RSC Adv.* **2023**, *13*, 6422−6432.
(50) Goncalves, G.; Marques, P. A. A. P.; Granadeiro, C. M.; Nogueira, H. I. S.; Singh, M. K.; Grácio, J. Surface Modification of Graphene Nanosheets with Gold Nanoparticles: The Role of Oxygen Moieties at Graphene Surface on Gold Nucleation and Growth. *Chem. Mater.* **2009**, *21*, 4796−4802.
(51) Hou, J.; Gao, X.; Bao, S.; Liu, S.; Yang, G. Yellow Emissive Nitrogen-doped Carbon Dots as a Fluorescence Probe for the Sensitive and Selective Detection of Silver Ions. *RSC Adv.* **2023**, *13*, 10508−10512.
(52) Kurniawan, D.; Chiang, W.-H. Microplasma-Enabled Colloidal Nitrogen-Doped Graphene Quantum Dots for Broad-Range FluorescENt pH Sensors. *Carbon* **2020**, *167*, 675−684.
(53) Khan, W. U.; Wang, D.; Zhang, W.; Tang, Z.; Ma, X.; Ding, X.; Du, S.; Wang, Y. High Quantum Yield Green-Emitting Carbon Dots for Fe(III) Detection, Biocompatible Fluorescent Ink and Cellular Imaging. *Sci. Rep.* **2017**, *7*, 14866.
(54) Gao, Z.; Lin, Z.; Chen, X.; Zhong, H.; Huang, Z. A Fluorescent Probe Based on N-doped Carbon Dots for Highly Sensitive Detection of Hg^{2+} in Aqueous Solutions. *Anal. Methods* **2016**, *8*, 2297−2304.
(55) Gu, S.; Hsieh, C.-T.; Yuan, C.-Y.; Ashraf Gandomi, Y.; Chang, J.-K.; Fu, C.-C.; Yang, J.-W.; Juang, R.-S. Fluorescence of Functionalized Graphene Quantum Dots Prepared from Infrared-Assisted Pyrolysis of Citric Acid and Urea. *J. Lumin.* **2020**, *217*, No. 116774.
(56) Terracina, A.; Armano, A.; Meloni, M.; Panniello, A.; Minervini, G.; Madonia, A.; Cannas, M.; Striccoli, M.; Malfatti, L.; Messina, F. Photobleaching and Recovery Kinetics of a Palette of Carbon Nanodots Probed by In Situ Optical Spectroscopy. *ACS Appl. Mater. Interfaces* **2022**, *14*, 36038−36051.
(57) Mura, S.; Ludmerczki, R.; Stagi, L.; Garroni, S.; Carbonaro, C. M.; Ricci, P. C.; Casula, M. F.; Malfatti, L.; Innocenzi, P. Integrating Sol-Gel and Carbon Dots Chemistry for the Fabrication of Fluorescent Hybrid Organic-Inorganic Films. *Sci. Rep.* **2020**, *10*, 4770.
(58) Khavlyuk, P. D.; Stepanidenko, E. A.; Bondarenko, D. P.; Danilov, D. V.; Koroleva, A. V.; Baranov, A. V.; Maslov, V. G.; Kasak, P.; Fedorov, A. V.; Ushakova, E. V.; Rogach, A. L. The Influence of Thermal Treatment Conditions (Solvothermal Versus Microwave) and Solvent Polarity on the Morphology and Emission of Phloroglucinol-based Nitrogen-Doped Carbon Dots. *Nanoscale* **2021**, *13*, 3070−3078.
(59) Zhang, Y.; Hu, Y.; Lin, J.; Fan, Y.; Li, Y.; Lv, Y.; Liu, X. Excitation Wavelength Independence: Toward Low-Threshold Amplified Spontaneous Emission from Carbon Nanodots. *ACS Appl. Mater. Interfaces* **2016**, *8*, 25454−25460.
(60) Forget, S.; Chenais, S. *Organic Solid-State Lasers*; SpringerVerlag: Berlin, 2013.
(61) Guzelturk, B.; Pelton, M.; Olutas, M.; Demir, H. V. Giant Modal Gain Coefficients in Colloidal II−VI Nanoplatelets. *Nano Lett.* **2019**, *19*, 277−282.
(62) Negro, L. D.; Bettotti, P.; Cazzanelli, M.; Pacifici, D.; Pavesi, L. Applicability Conditions and Experimental Analysis of the Variable Stripe Length Method for Gain Measurements. *Opt. Commun.* **2004**, *229*, 337−348.
(63) Ibnaouf, K. H.; Taha, K. K.; Idriss, H.; Aldaghri, O. Amplified Spontaneous Emission (ASE) Properties of a Laser Dye (LD-473) in Solid State. *J. Eur. Opt. Soc. Rapid Publ.* **2017**, *13*, 20.
(64) van der Molen, K. L.; Mosk, A. P.; Lagendijk, A. Quantitative Analysis of Several Random Lasers. *Opt. Commun.* **2007**, *278*, 110−113.
(65) Tang, L.; Ai, L.; Song, Z.; Sui, L.; Yu, J.; Yang, X.; Song, H.; Zhang, B.; Hu, Y.; Zhang, Y.; Tian, Y.; Lu, S. Acid-Triggered Aggregation of Carbon Dots Shifted Their Emission to Give Unexpected Deep-Red Lasing. *Adv. Funct. Mater.* **2023**, *33*, 2303363.
(66) Qu, S.; Liu, X.; Guo, X.; Chu, M.; Zhang, L.; Shen, D. Amplified Spontaneous Green Emission and Lasing Emission from Carbon Nanoparticles. *Adv. Funct. Mater.* **2014**, *24*, 2689−2695.
(67) Bian, Y.; Shi, X.; Hu, M.; Wang, Z. A Ring-Shaped Random Laser in Momentum Space. *Nanoscale* **2020**, *12*, 3166−3173.
(68) Ghasempour Ardakani, A.; Shahvandpour, M. A Simple Method to Achieve a Directional and Resonant Random Lasing Emission Using Graphene Quantum Dots as Scattering Elements. *Phys. B Condens. Matter* **2021**, *616*, No. 413133.
(69) Tenopala-Carmona, F.; García-Segundo, C.; Cuando-Espitia, N.; Hernández-Cordero, J. Angular Distribution of Random Laser Emission. *Opt. Lett.* **2014**, *39*, 655−658.
(70) Ghofraniha, N.; Viola, I.; Dimaria, F.; Barbarella, G.; Gigli, G.; Leuzzi, L.; Conti, C. Experimental Evidence of Replica Symmetry Breaking in Random Lasers. *Nat. Commun.* **2015**, *6*, 6058.
(71) Moura, A. L.; Pincheira, P. I. R.; Reyna, A. S.; Raposo, E. P.; Gomes, A. S. L.; de Araújo, C. B. Replica Symmetry Breaking in the Photonic Ferromagneticlike Spontaneous Mode-Locking Phase of a Multimode Nd:YAG Laser. *Phys. Rev. Lett.* **2017**, *119*, No. 163902.
(72) Fallert, J.; Dietz, R. J. B.; Sartor, J.; Schneider, D.; Klingshirn, C.; Kalt, H. Co-existence of Strongly and Weakly Localized Random Laser Modes. *Nat. Photonics* **2009**, *3*, 279−282.
(73) Mujumdar, S.; Türck, V.; Torre, R.; Wiersma, D. S. Chaotic Behavior of a Random Laser with Static Disorder. *Phys. Rev. A* **2007**, *76*, 33807.
(74) Chen, Y.; Herrnsdorf, J.; Guilhabert, B.; Zhang, Y.; Watson, I. M.; Gu, E.; Laurand, N.; Dawson, M. D. Colloidal quantum dot random laser. *Opt. Express* **2011**, *19*, 2996−3003.
(75) Sarkar, A.; Bhaktha, B. N. S.; Andreasen, J. Replica Symmetry Breaking in a Weakly Scattering Optofluidic Random Laser. *Sci. Rep.* **2020**, *10*, 2628.
(76) Sznitko, L.; Cyprych, K.; Szukalski, A.; Miniewicz, A.; Mysliwiec, J. Coherent−incoherent random lasing based on nanorubbing induced cavities. *Laser Phys. Lett.* **2014**, *11*, 45801.
(77) Xia, J.; Xie, K.; Ma, J.; Chen, X.; Li, Y.; Wen, J.; Chen, J.; Zhang, J.; Wu, S.; Cheng, X.; Hu, Z. The Transition from Incoherent to Coherent Random Laser in Defect Waveguide Based on Organic/Inorganic Hybrid Laser Dye. *Nanophotonics* **2018**, *7*, 1341−1350.
(78) Ejbarah, R. A.; Jassim, J. M.; Haddawi, S. F.; Hamidi, S. M. Transition from Incoherent to Coherent Random Lasing by Adjusting Silver Nanowires. *Appl. Phys. A* **2021**, *127*, 476.
(79) Ito, T.; Tomita, M. Analysis of Gain Volume in Random Laser in a Spherical Multiple Scattering Medium. *Opt. Rev.* **2004**, *11*, 7−11.
(80) Wang, Z.; Shi, X.; Wei, S.; Sun, Y.; Wang, Y.; Zhou, J.; Shi, J.; Liu, D. Two-threshold Silver Nanowire-based Random Laser with Different Dye Concentrations. *Laser Phys. Lett.* **2014**, *11*, 95002.
(81) Choubey, P. S.; Sarkar, A.; Varshney, S. K.; BN, S. B. Random Laser Spectroscopy and Replica Symmetry Breaking Phase Transitions in a Solvent-rich Polymer Thin Film Waveguide. *J. Opt. Soc. Am. B* **2020**, *37*, 2505−2513.
(82) Merrill, J. W.; Cao, H.; Dufresne, E. R. Fluctuations and Correlations of Emission from Random Lasers. *Phys. Rev. A* **2016**, *93*, 21801.
(83) Abaie, B.; Mobini, E.; Karbasi, S.; Hawkins, T.; Ballato, J.; Mafi, A. Random Lasing in an Anderson Localizing Optical Fiber. *Light Sci. Appl.* **2017**, *6*, No. e17041.
(84) Jimenez-Villar, E.; da Silva, I. F.; Mestre, V.; Wetter, N. U.; Lopez, C.; de Oliveira, P. C.; Faustino, W. M.; de Sa, G. F. Random Lasing at Localization Transition in a Colloidal Suspension (TiO2@Silica). *ACS Omega* **2017**, *2*, 2415−2421.
(85) He, J.; Chan, W.-K.; Cheng, X.; Tse, M.-L.; Lu, C.; Wai, P.-K.; Savovic, S.; Tam, H.-Y. Experimental and Theoretical Investigation of the Polymer Optical Fiber Random Laser with Resonant Feedback. *Adv. Opt. Mater.* **2018**, *6*, 1701187−1701195.

https://doi.org/10.1021/acsphotonics.4c00279
ACS Photonics XXXX, XXX, XXX−XXX

(86) Li, J.; Li, X.; Li, Y.; Sang, Y.; Zheng, T.; Liu, J.; Liu, M.; Hu, S.; Guo, J. Dual-band Random Laser Based on Positive Replica of Abalone Shell. *J. Lumin.* **2022**, *241*, No. 118543.
(87) Wang, Y.-C.; Li, H.; Hong, Y.-H.; Hong, K.-B.; Chen, F.-C.; Hsu, C.-H.; Lee, R.-K.; Conti, C.; Kao, T. S.; Lu, T.-C. Flexible Organometal−Halide Perovskite Lasers for Speckle Reduction in Imaging Projection. *ACS Nano* **2019**, *13*, 5421−5429.

https://doi.org/10.1021/acsphotonics.4c00279
ACS Photonics XXXX, XXX, XXX−XXX